Nanotechnology

LETTER

Fabrication of arrays of tapered silicon micro-/nano-pillars by metal-assisted chemical etching and anisotropic wet etching

To cite this article: K Yamada *et al* 2018 *Nanotechnology* **29** 28LT01

View the article online for updates and enhancements.

Related content

- Vertical Si nanowire arrays fabricated by magnetically guided metal-assisted chemical etching
Dong Won Chun, Tae Kyoung Kim, Duyoung Choi et al.

- Nanostructured silicon via metal assisted catalyzed etch (MACE): chemistry fundamentals and pattern engineering
Fatima Toor, Jeffrey B Miller, Lauren M Davidson et al.

- Advanced fabrication of Si nanowire FET structures by means of a parallel approach
J Li, S Pud, D Mayer et al.

This content was downloaded from IP address 131.113.64.219 on 28/05/2018 at 02:59

IOP Publishing
Letters
Nanotechnology
Nanotechnology **29** (2018) 28LT01 (9pp)
https://doi.org/10.1088/1361-6528/aac04b

Letter

Fabrication of arrays of tapered silicon micro-/nano-pillars by metal-assisted chemical etching and anisotropic wet etching

K Yamada, M Yamada, H Maki and K M Itoh

School of Fundamental Science and Technology, Keio University, Yokohama 223-8522, Japan

E-mail: kitoh@appi.keio.ac.jp

Received 23 March 2018, revised 10 April 2018
Accepted for publication 26 April 2018
Published 11 May 2018

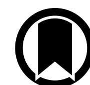

Abstract

Fabrication of a 2D square lattice array of intentionally tapered micro-/nano-silicon pillars by metal-assisted chemical etching (MACE) of silicon wafers is reported. The pillars are square rod shaped with the cross-sections in the range 0.2 × 0.2–0.9 × 0.9 μm^2 and heights 3–7 μm. The spacing between pillars in the 2D square lattice was controlled between 0.5 and 3.0 μm. While the pillars after MACE had the high aspect ratio ∼1:5, subsequent anisotropic wet etching in potassium hydroxide solution led to 80°–89.5° tapers with smooth sidewalls. The resulting taper angle showed the relation with geometry of pillar structures; the spacing 0.5–3.0 μm led to the tapering angle 89.5°–80° for 3 and 5 μm tall pillars but 7 μm tall pillars showed no dependency between the tapering angle and the inter-pillar spacing. Such an array of silicon tapered-rods with smooth sidewalls is expected to be applicable as a mold in nanoimprinting applications.

Keywords: metal-assisted chemical etching, anisotropic wet etching, silicon nanowire, nanoimprint

(Some figures may appear in colour only in the online journal)

1. Introduction

A mold profile in nanoimprint lithography (NIL) [1–3] plays a significant role. NIL is capable of patterning from sub-10 nm to sub-micron structures with high-throughput as well as at the low cost owing to the advantage that the NIL mold can be reused repeatedly [4–12]. In order to make the NIL mold durable, de-molding force, which is a force required to separate the mold from the resist after replicating patterns needs to be minimized. The small de-molding force also helps to reduce the number of defects on the transferred pattern. Although antiadhesive coatings with fluorinated silane are often used for easy mold releasing [13], the exact profile of mold is also important. Especially, smooth and tapering (less than 90°) sidewalls are necessary for easy de-molding. High aspect ratios (diameter:height) of 1:5 are typically demanded for well define imprinting [14–19]. Silicon (Si) wafers have been popular choice as the mold platform for applications like the patterned media and optical films that are typically composed of the sub-micron diameter 2D lattice pattern. The electron beam lithography followed by reactive ion etching is the standard procedure to fabricate sub-micron mold patterns on Si wafers. In particular, Bosch process is employed to fabricate high aspect ratio structures [20–22]. However, even with Bosch process, obtaining smooth side wall is not straightforward. While it is possible to control taper angles by adjusting flow rate of etching gas [23], a sidewall ripple called scalloping is emerged at the time of switching between the etching and protection gases [20, 21]. Some efforts have been devoted to reduce the scalloping, e.g., by introducing O_2 gas

 © 2018 IOP Publishing Ltd Printed in the UK

into etching gas [14], decreasing the etching rate, and etching with alkaline solutions [15]. However, complete removing of scalloping has not been achieved to our knowledge.

Metal-assisted chemical etching (MACE) has attracted much attention in recent years as an inexpensive, high-throughput wet etching method that can fabricate high aspect ratio structures with smooth sidewalls [24–28]. In MACE, metals (e.g. Ag, Au, and Pt) deposited on the Si substrate play a role of catalyst when being immersed in mixture of hydrofluoric acid (HF) and hydrogen peroxide (H_2O_2). Si that is in contact with the metal is oxidized by electrochemical reaction and subsequent HF etching removes SiO_2. This process is very fast that the sidewall etching is very limited leading to smooth sidewalls. The uniformity of etching can be improved by inserting Fe layer into Au layers as Au/Fe/Au and apply externally magnetic field during etching to improve the metal-silicon adhesion [29]. However, by MACE alone, only vertical (almost 90° to substrate) structures can be fabricated.

In this paper, we demonstrate an experimental technique to fabricate tapering structures employing combination of MACE followed by another wet etching by potassium hydroxide solution (KOH). KOH etching has been known to expose Si (111) surface [30–33]. Indeed, such a sharpening protocol with KOH has been employed in the past to reveal 54.7° (111) surfaces at the top of Si micro-/nano-structures [34–36]. However, despite four equivalent (111) planes having the angle 54.7° to the (100) surface of Si wafer employed in this study, we have achieved the control of the angle in the range between 80° and 89.5°. The key finding, as we will show, is the geometric factor of the nanorod can change the tapering angle of sidewall etching by KOH.

2. Experimental

Figure 1 shows the experimental steps. Starting substrate was a 525 μm thick float-zone n-type Si (100) wafer having the resistivity of 2000 Ω cm. The wafer was cleaved into 20 × 20 mm pieces. The samples were cleaned by ultra-sonication in acetone for 10 min. The electron beam resist (ZEON ZEP 520A) was coated by a spin coater in two steps; 1000 rpm for 5 s followed by 3000 rpm for 50 s. The 2D square array mask pattern was drawn by electron beam lithography (20 kV, 56 μC cm^{-2}) followed by a positive resist developing. Four layers of metals, 5 nm Ti/10 nm Au/10 nm Fe/10 nm Au, were deposited in a high vacuum evaporator. Without lifting off the resist, MACE of the sample was performed in HF/H_2O_2 (45% HF:30% H_2O_2 = 8:2) in a Teflon beaker placed on a neodymium magnet (188 mT cm^{-2}) at room temperature in a non-clean room, i.e., in a regular chemical lab environment. The samples were immersed for 3 min with the metal film side facing upward. During this process, the region under the Si surface (more precisely SiO_2 surface) that was in direct contact with the Ti layer was oxidized preferentially and etched away. However, the Ti/Au/Fe/Au film continues to stick to the Si interface even when SiO_2 at the interface was removed. As a result, the metal pattern continues to sink into Si bulk with the rate of about 5 μm in 3 min. On the other hand, the silicon surface region that was not in direct contact with the metal films was not etched. In the present case, even though we did not perform the electron beam resist lift-off before MACE, the region that had electron beam resist between the Si and metal films remained unetched. Therefore, the resulting pillars after MACE had the stack of the electron beam resist and metal films at the top, while the valley floor was covered entirely by the metal films only. These remaining metal films and

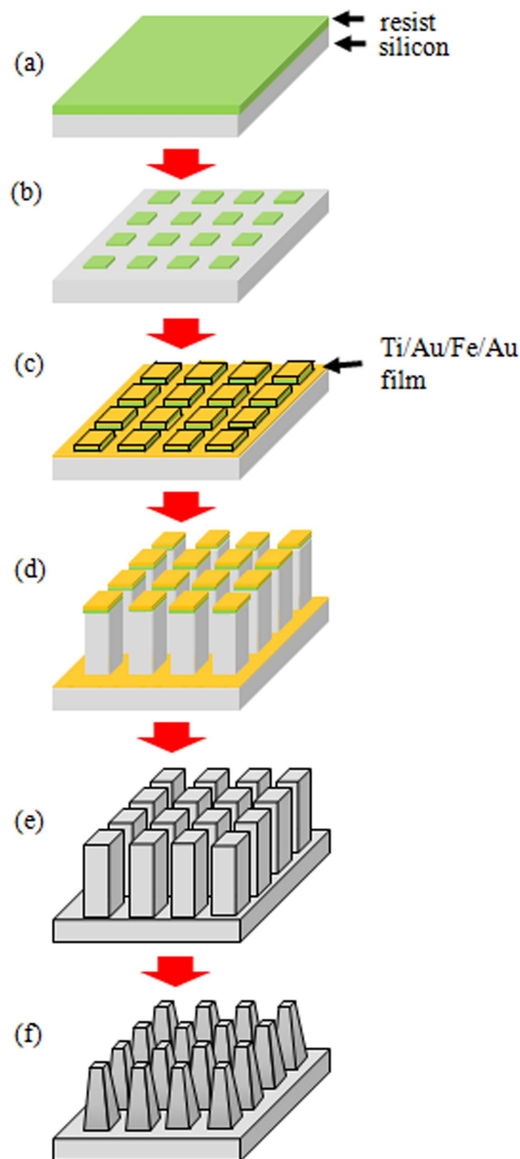

Figure 1. Five major steps of the present experiment. (a) Surface coating of the Si sample by the electron beam resists ZEP 520 A. (b) Patterning of the squares array lattice by the electron beam lithography. The green squares show the remaining resists. (c) Vacuum deposition of Ti, Au, Fe, and Au layers in sequence. 5 nm Ti/10 nm Au/10 nm Fe/10 nm Au. (d) Metal-assisted chemical etching by immersing the sample in a solution composed of 45% HF:30% H_2O_2 = 8:2. A permanent magnet is placed under the etching beaker as the magnetic force guide to enhance the adhesion between the metal and silicon. (e) Removal of the metal and resist films by nitrohydrochloric acid and dichloromethane. (f) Anisotropic etching for 10 s in KOH (3 mol l^{-1}) for tapering of the sidewalls.

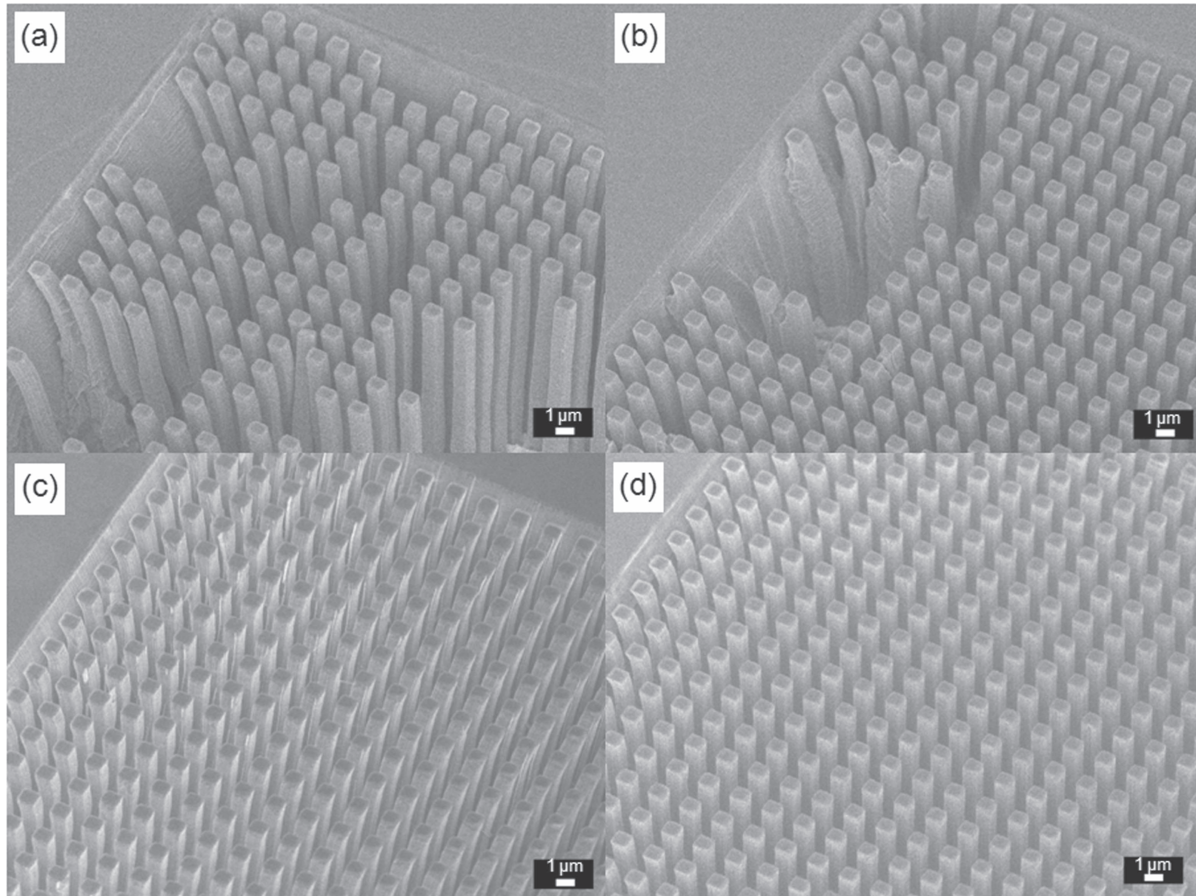

Figure 2. Scanning electron micrographs (SEM) demonstrating the effects of the insertion of the Fe layer and placing the permanent magnet at the bottom of the beaker, i.e., the magnetic force guide, during MACE. (a) MACE with the 5 nm Ti/10 nm Au layers without the magnetic force guide for 3 min, (b) MACE with the 5 nm Ti/10 nm Au layers with the magnetic force guide for 3 min, (c) MACE with the 5 nm Ti/10 nm Au/10 nm Fe/10 nm Au layers without the magnetic force guide for 7 min, and (d) MACE with the 5 nm Ti/10 nm Au/10 nm Fe/10 nm Au layers with the magnetic force guide for 7 min. The scale bar in each photo shows 1 μm.

electron beam resist were removed by immersing the sample in nitrohydrochloric acid and dichloromethane in sequence. Finally, the vertical sidewalls of the pillars are slanted by immersing the sample in KOH (3 mol l^{-1}) alkaline solution for 10 s at room temperature. A JEOL JSM-7600F scanning electron microscope (SEM) was used for observation of the sample structures.

While the above-mentioned procedure led to the optimum resulting structures, in order to show the advantage of having the Fe layer, we have also performed MACE with the 5 nm Ti/10 nm Au layers. Moreover, as discussed in below, we have also performed MACE without placing the magnet beneath the beaker.

3. Results and discussion

First, we evaluated the effect of magnetic force guide for the improvement of MACE uniformity. Figure 2 shows a comparison of (a) MACE with Ti/Au films without magnetic force guide for 3 min, (b) MACE with Ti/Au films with magnetic force guide for 3 min, (c) MACE with Ti/Au/Fe/Au films without magnetic force guide for 7 min, and (d) MACE with Ti/Au/Fe/Au with magnetic force guide for 7 min. The difference in MACE times, 3 and 7 min, was selected to obtain approximately the same etching rates; the MACE with Fe having the thicker overlayer having the etching rate of $\sim$1.3 μm min^{-1} was slower than $\sim$3.0 μm min^{-1} with the thinner Ti/Au overlayers. As seen in figure 2, the resulting structure with Ti/Au/Fe/Au contains smaller number of defects than the ones with Ti/Au. Here the etching speed with Ti/Au appeared to be too fast. When compared between with and without magnetic force for Ti/Au/Fe/Au (figures 2(c) and (d)), a subtle difference appears in the spatial homogeneity in the etching speed. Figure 3 shows the pillar length variation using the constant height contour lines when the magnet was not placed under the beaker during MACE using Ti/Au/Fe/Au, i.e., same as figure 2(c). Within the shown area of 50 $\times$ 50 μm^2, the height variation of a few micron was observed. On the other hand, the Si pillars fabricated by MACE with Ti/Au/Fe/Au with magnetic force guide shown in figure 4 are highly uniform (sub-micron height variation) in 70 $\times$ 80 pillars. Two defects indicated by ‘a’ and two gold flakes indicated by ‘b’ are seen corresponding to defect fraction of 0.04% only and they should be eliminated further by performing the entire process in a clean room.

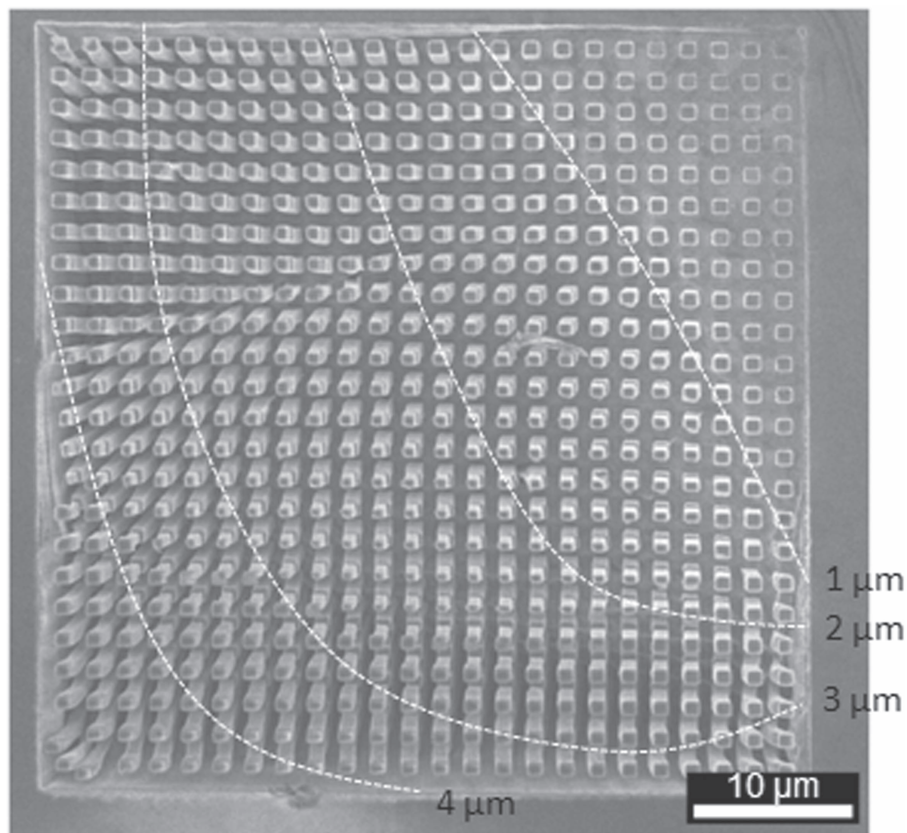

Figure 3. SEM of the Si pillar array fabricated by MACE with Ti/Au/Fe/Au without magnetic force guide. Each dot line represents the contour line of the pillar height. MACE without magnetic force guide leads to macroscopic inhomogeneity in the pillar height.

We shall now analyze the observed results by revisiting the MACE mechanism. A schematic of MACE reaction is shown in figure 5. The important step of MACE is the hole injection into Si through the metal catalyst followed by oxidization of Si. These holes are provided by the oxidant H_2O_2. SiO_2 oxidized from Si by accepting holes can be dissolved by HF from the edges of films but the noble metal films continue to stick to the etched Si bare surface [37]. By keeping these reactions, the metal catalyst sinks deeply into the substrate. Since this is an electrochemical reaction, the type of metals used as a catalyst plays an important role to transfer the holes into Si [38–40]. Concretely, the electronegativity of catalyst metals is considered to be controlling physical parameters [41]. When the electronegativity of the metal is higher than that of Si, it is easier for Si to accept holes to speed up the MACE process. Therefore, noble metals usually employed for MACE such as Au, Ag, or Pt have high electronegativity but these metals do not adhere to Si very strongly and tend to peel off during MACE. Thus, a thin Ti layer is often employed to sustain the adhesion with Si [42, 43]. Although electronegativity of Ti is lower than that of Si, MACE proceeds when Ti between Si and Au is less than 5 nm. Therefore, Ti/Au layers can act as good catalysts in MACE. Moreover, since holes diffuse isotropically into Si, oxidation of Si proceeds isotropically from the center of the metal areas. As a result, it is often observed that an etching direction strays away from the vertical direction [42, 43]. This phenomenon is assumed as the reason why the variation of the pillars' length is caused in the absence of magnetic field guide and the inserted magnetic layer. In the case of our experiment, since the metal catalysts are 2D mesh patterns, such effect appeared as the difference in the etching speed in a large area. However, magnetically guided MACE can also improve this directionality in addition to the etching speed spatial uniformity [29]. In the present experiment, the permanent magnet was placed under the Teflon beaker to force the Fe magnetic layers to the vertical direction. Moreover the magnetic force enhances the adhesion of catalysts and Si. Thus, in this study, the combination of Ti/Au/Fe/Au and magnetic force guide led to the stable metal adhesion to Si and high uniformity.

Magnified SEM images of Si pillar arrays fabricated by magnetically guided MACE are shown in figure 6. Here the cross-section of each pillar is $1 \times 1\ \mu m^2$ and height is $\sim 5\ \mu m$. The spacing between pillars was varied between 0.5 and $3.0\ \mu m$. Completely vertical sidewalls having fairly smooth surfaces were obtained in all cases. The structures shown in figure 6 are then immersed in KOH etching solution to add desired tappers as shown in figure 7. figures 7(a1)–(f1) show that the sidewalls of each pillar were uniformly tapered while maintaining the fairly smooth surface morphology. The change in the area of the top of the pillars from $0.9 \times 0.9\ \mu m^2$ of figures 7(a1) and (a2) to $0.2 \times 0.2\ \mu m^2$ of figures 7(f1) and (f2), while maintaining the same cross-section at the bottom, demonstrate that the change in the tapering angles. What is remarkable here is that although KOH anisotropic etching

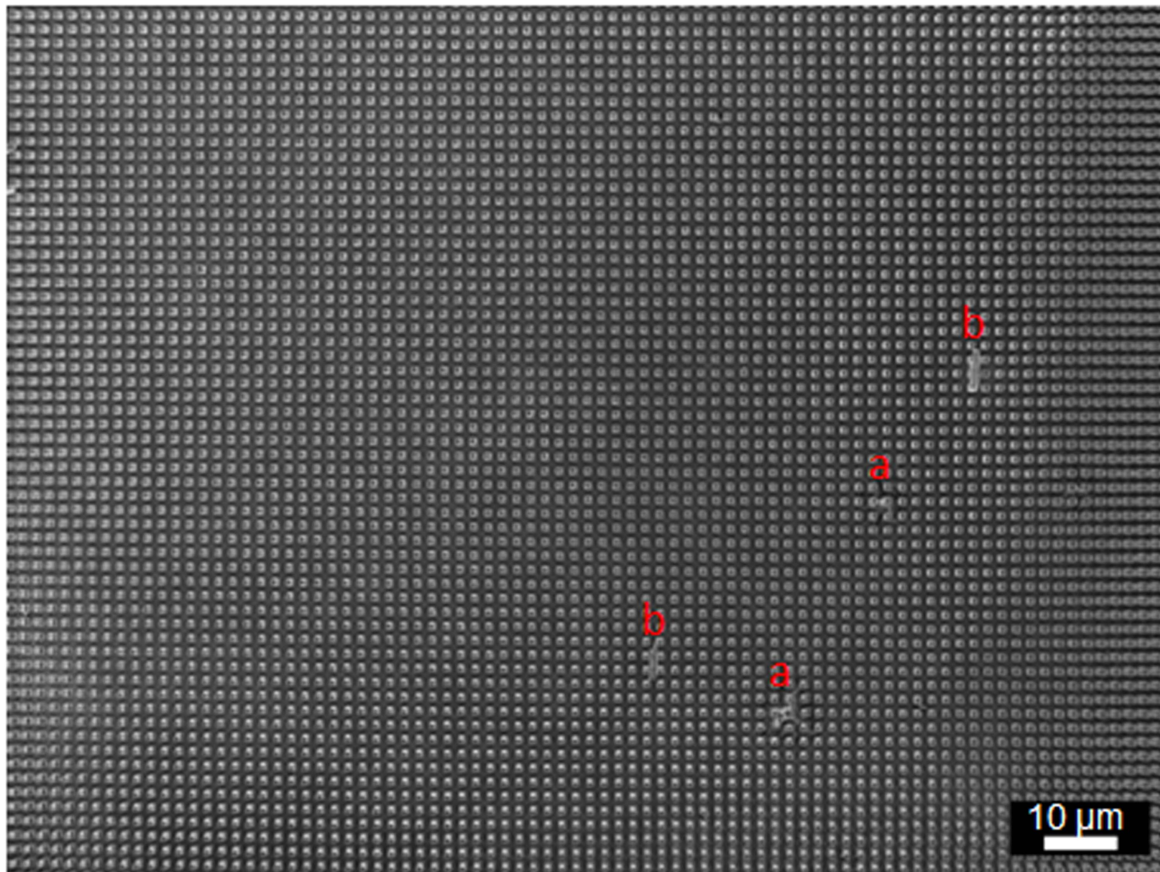

Figure 4. A typical SEM of the very homogeneous Si pillar array fabricated by MACE with the 5 nm Ti/10 nm Au/10 nm Fe/10 nm Au layers with the magnetic force guide. 1×1 μm^2 square cross-section pillars with the spacing of 1 μm and uniform height of 5 μm were fabricated in the observed area of 140×160 μm^2. Two defects indicated by 'a' and two gold flakes indicated by 'b' are seen corresponding to defect fraction of 0.04%.

was supposed to reveal (111) facets that have the angle of 54.7° to the Si surfaces, the tapering angles as determined from figures 7(a1)–(f1) are much larger, in the range of 80°–89.5°.

In order to understand such rather unexpected phenomenon, we first point out the feature that the pillar cross-sections remain squares for every pillar before and after KOH etching; only the tapering angles change. Calculation from the resulting tapering angles indicates that (441) surface has been appeared in the case of 80° tapers. Considering that Si surface atoms having two dangling bonds, i.e., Si (100) and (110) surfaces, are easier to bond with OH^- ions than ones having only one dangling bond, the alkaline solution etches Si (100) and (110) preferentially resulting in the square cross-sections everywhere. The same principle applies to the other surfaces such as (411) [44].

The question remains why (111) surfaces were not exposed by KOH. First obvious possibility is that 10 s etching time by KOH was not long enough to expose 54.7° surfaces. When the bottom cross-section is 1×1 μm^2 square, the expected heights of Si pyramids with 54.7° (111) surfaces is ~0.7 μm. The longer etching time may expose pyramid at the top of each pillar. However, even when we varied the etching time in KOH up to 10 s and longer, the taper angles shown in figure 7 were maintained. The structures simply became smaller by the longer etching time keeping the maximum angle. In order to further investigate the anisotropy of the KOH etching on Si pillars, we performed the KOH etching on 45° rotated Si pillars, i.e., the ones having four surfaces having the (100) orientations. If the anisotropy of the KOH etching appears, each edge of pillars should be rounded or etched away leading to circular or octagonal pillars. However, as shown in figure 8, the etching anisotropy did not change between (100) and (110) sidewalls. Therefore the unexpected tapering phenomena observed in this study cannot be explained by simple anisotropy of KOH etching.

The most plausible cause we presently believe is the change in the ability for the KOH etching solution to flow into the inter-pillar regions (volumes), which can be affected strongly by the inter-pillar spacing and pillar heights. It is well known that hydrogen gas is generated as a result of chemical reaction between KOH and Si. Such generated hydrogen gas can be trapped between sidewalls of adjacent pillars and prevent KOH solution reaching in inter-pillar regions. Such coexistence of hydrogen gas and KOH solution between pillars may reduce the anisotropic etching character of KOH and result in rather averaged out uniform etching leading to flat sidewalls with much larger taper angle than 54.7°. In order to verify this, we also performed the KOH etching on 3 and 7 μm Si pillar arrays whose inter-pillar spacings are

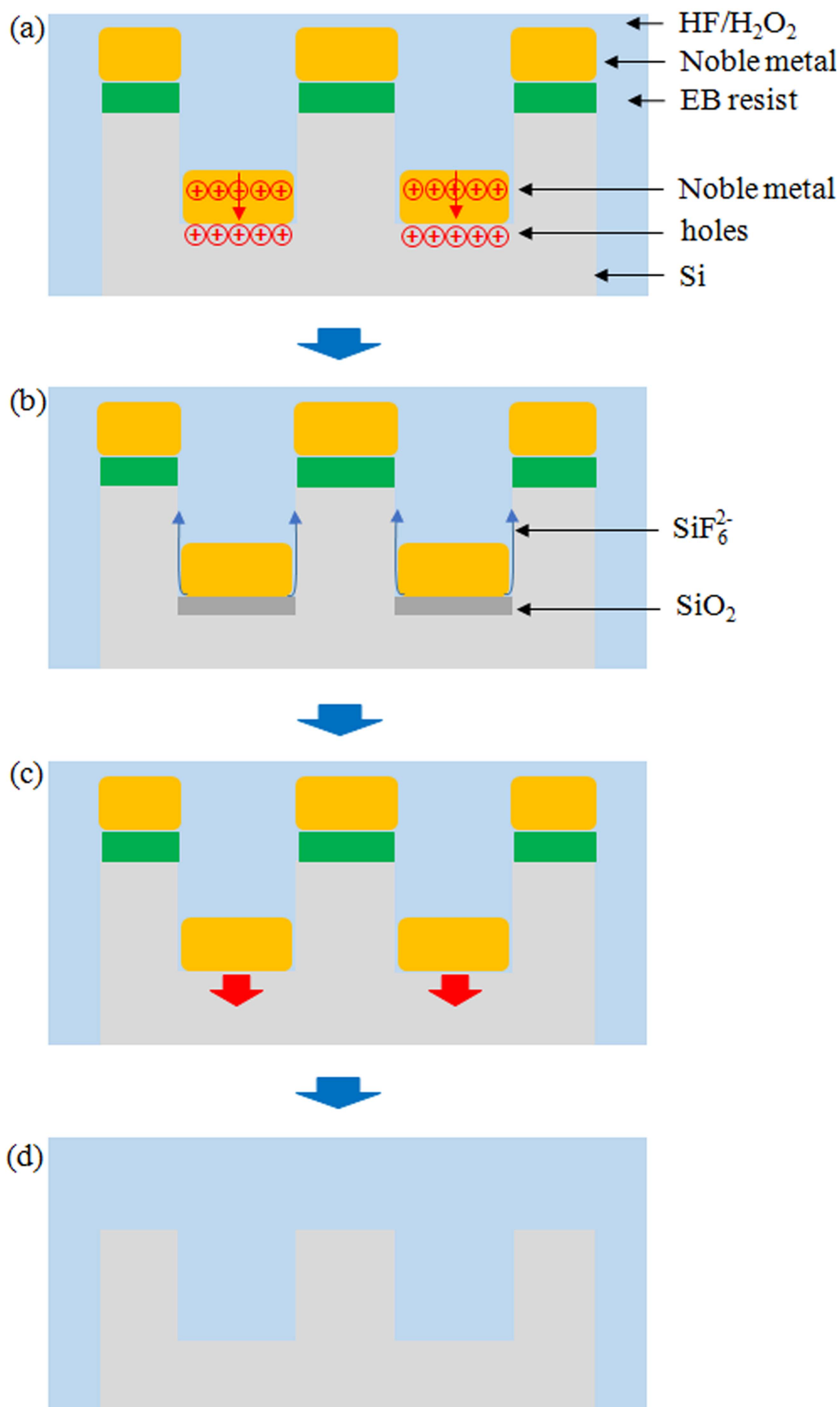

Figure 5. A schematic of MACE reaction. (a) Hole diffusion and oxidation of Si by H_2O_2 via the noble metal films deposited on the Si substrate. (b) SiO_2 etching by HF solution from the edges of noble metal films and dissolving of SiO_2 into SiF_6^{2-}. (c) Sticking of the noble metal films to the exposed Si surface leading to the 'local sinking,' i.e., local etching of the valley floor. (d) Removal of the noble metal and photoresist films by nitrohydrochloric acid and dichloromethane.

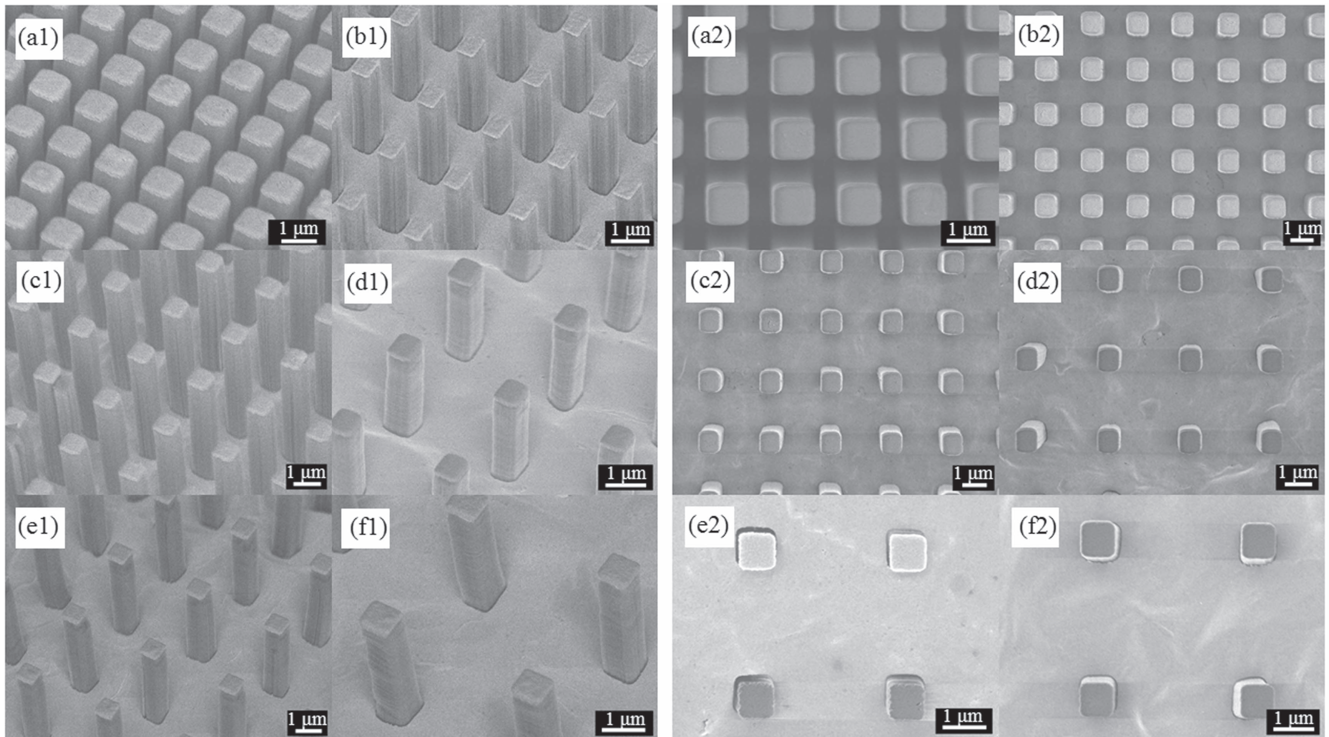

Figure 6. SEM images of the Si pillar 2D square lattice arrays fabricated by the magnetically guided MACE. The cross-section of each pillar is $1 \times 1\ \mu m^2$ and the height is $\sim$5 μm. The inter-pillar spacings are (a1), (a2) 0.5 μm, (b1), (b2) 1.0 μm, (c1), (c2) 1.5 μm, (d1), (d2) 2.0 μm, (e1), (e2) 2.5 μm, and (f1), (f2) 3.0 μm. (a1)–(f1) are images taken with the 40° tilt from the vertical direction and (a2)–(f2) are images taken from top.

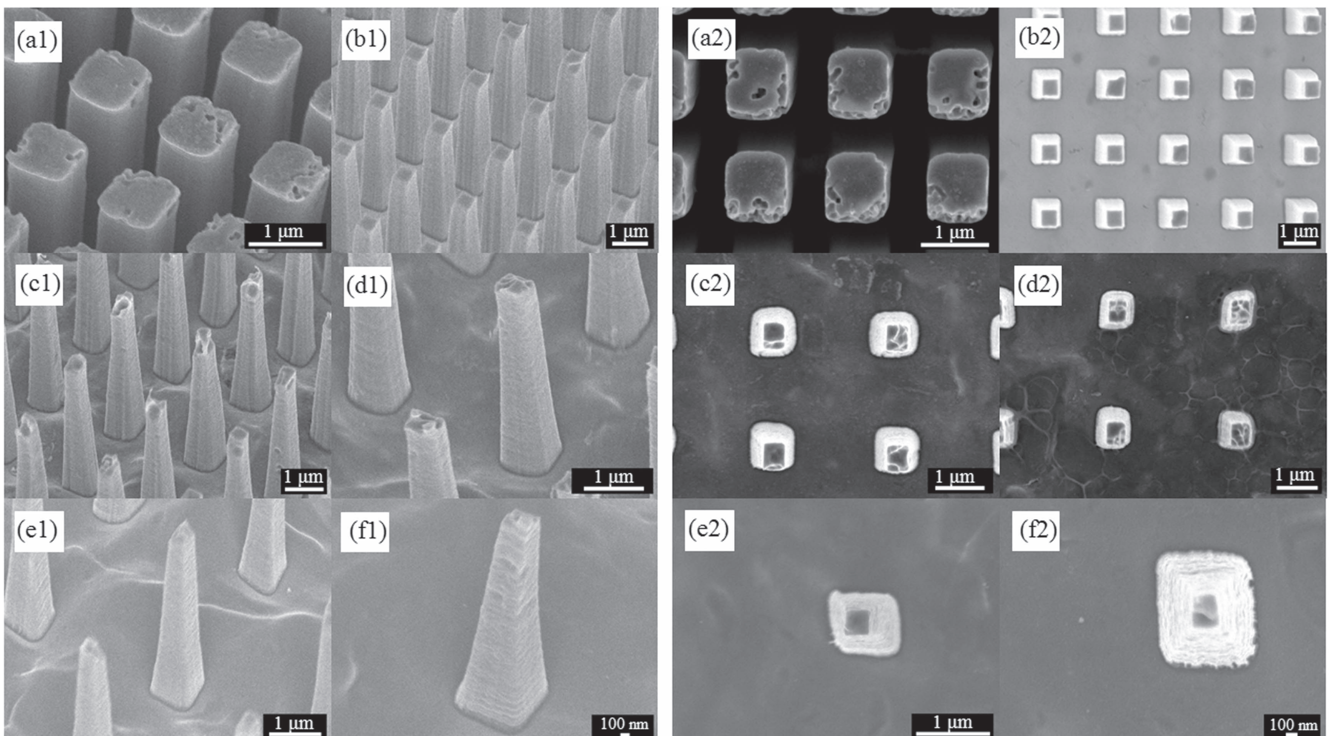

Figure 7. SEM images of the Si pillar 2D square lattice arrays shown in figure 6 tapered by the anisotropic wet etching by the KOH solution. The inter-pillar spacings are (a1), (a2) 0.5 μm, (b1), (b2) 1.0 μm, (c1), (c2) 1.5 μm, (d1), (d2) 2.0 μm, (e1), (e2) 2.5 μm, and (f1), (f2) 3.0 μm. (a1)–(f1) are images taken with the 40° tilt from the vertical direction and (a2)–(f2) are images taken from top.

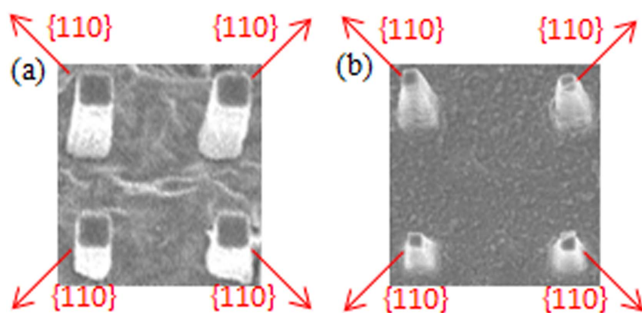

Figure 8. The SEMs showing the effect of the in-plane crystallographic orientation on the tapering by the KOH solution. Red arrows show orientations of the in-plane ⟨110⟩ directions that should be etched preferentially by the anisotropic etching by KOH. However, above images (a) and (b) indicate that the KOH etching in the present case does not show apparent anisotropy.

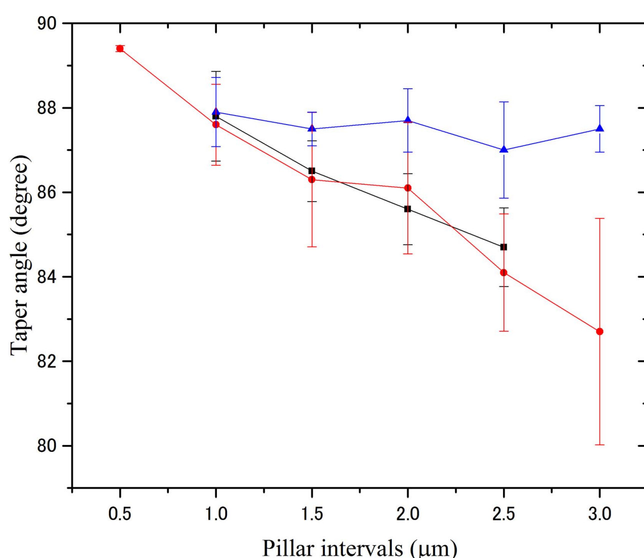

Figure 9. The taper angle of the Si pillars in the 2D square lattice arrays as a function of the inter-pillar spacing. Short Si pillars whose heights are 3 μm (■) and 5 μm (•) show the dependency between taper angle and pillar intervals, while long pillars having 7 μm heights (▲) show no dependency.

controlled between 0.5 and 3.0 μm. The results are shown in figure 9. Error bars represent the variation in the taper angles within which 95% of pillars measured for the given spacing resulted. Interestingly, in the case of 3 and 5 μm pillars, the larger the inter-pillar spacing is, the smaller the taper angle becomes. In the case of 7 μm pillars, taper angles show no dependence to the inter-pillar spacing. These experimental results indicate that geometrical factors, i.e., high aspect ratios combined with pillar spacing affect tapering angle by KOH etching as well as inter-pillar spacing.

In addition, the effects of Ti, Au, and Fe on KOH etching should be considered. In the previous report by H Tanaka *et al* even a small amount of metal ions in KOH solution can affect the etching property [45, 46]. However, their conclusion is that Ti, Au, and Fe, the metals used in our experiments, do not affect KOH etching property. The reason why the sidewalls of pillars shown in figure 7(f1) is slightly roughened by KOH etching is not clear. In general, the sidewall roughness after KOH appear to increase with increasing the inter-pillar spacing. The etching rate by KOH solution increases with the inter-pillar spacing especially for the case of 5 μm tall pillars. The sidewall roughness control for the KOH etching requires optimal balancing of the pillar height and inter-pillar spacing. Moreover, it is needed to investigate the effect of the concentration of the KOH solution as the additional freedom. It appears that, it is preferred to employ a high (>40 wt%) concentration KOH solution for reducing the surface roughness. In addition to the sidewall roughness, the pore structures were caused on the top surface of the Si pillars in figures 7(a1), (c1)–(f1). Generally, roughness on the top surface of the imprinting mold are not critical for the easy de-molding. These pore-like defects are considered as etching pits arose from the original lattice defects on Si pillars before the KOH etching and can also be removed by the optimal etching condition as figure 7(b1) shows.

In conclusion, fabrication of Si pillars with smooth and tapered sidewalls has been realized by combination of MACE and KOH etching. This technology can not only reduce the cost of production but can also fabricate smoother sidewalls on Si pillars in a short time. Rather unexpected behavior of KOH etching on high aspect ratio pillars observed in the present study was attributed to the presence of unescaped hydrogen bubbles around the sidewalls whose concentration is affected by the pillar height and inter-pillar spacing. In the future, it will be interesting to establish a look up table showing the relation between the inter-pillar spacing, pillars heights and resulting taper angle to develop a universal taper angling technique based on this simple wet etching method.

Acknowledgments

The authors thank Makoto Kuroda and Yasuo Komukai for the technical assistance. This was supported in parts by the Grant-in-Aid for Scientific Research by MEXT, Spin-RNJ, JSPS Core-to-Core Program, and Cooperative Research Project Program of the RIEC, Tohoku University.

ORCID iDs

K Yamada https://orcid.org/0000-0003-4413-6340

References

[1] Chou S Y, Krauss P R and Renstrom P J 1995 *Appl. Phys. Lett.* **67** 3114
[2] Chou S Y, Krauss P R and Renstrom P J 1996 *Science* **272** 85
[3] Chou S Y 1996 *J. Vac. Sci. Technol.* B **14** 4129
[4] Xia Q and Chou S Y 2008 *Nanotechnology* **19** 455301
[5] Li M, Wang J, Zhuang L and Chou S Y 2000 *Appl. Phys. Lett.* **76** 673
[6] Guo L J, Krauss P R and Chou S Y 1997 *Appl. Phys. Lett.* **71** 1881
[7] Jung G Y *et al* 2006 *Nano Lett.* **6** 351

[8] Guo L J 2004 *J. Phys. D: Appl. Phys.* **37** R123
[9] Guo L J 2007 *Adv. Mater.* **19** 495
[10] Schift H 2008 *J. Vac. Sci. Technol.* B **26** 458
[11] Dobisz E A, Bandić Z Z, Wu T W and Albrecht T 2008 *Proc. IEEE* **96** 1836
[12] Han K S, Shin J H, Yoon W Y and Lee H 2011 *Sol. Energy Mater. Sol. Cells* **95** 288
[13] Bailey T, Choi B J, Colburn M, Meissl M, Shaya S, Ekerdt J G, Sreenivasan S V and Willson C G 2000 *J. Vac. Sci. Technol.* B **18** 3572
[14] Kawata H, Yasuda M and Hirai Y 2006 *Japan. J. Appl. Phys.* **45** 5597
[15] Kawata H, Matsue M, Kubo K, Yasuda M and Hirai Y 2009 *Microelectron. Eng.* **86** 700
[16] Kawata H, Kubo K, Watanabe Y, Sakamoto J, Yasuda M and Hirai Y 2010 *Japan. J. Appl. Phys.* **49** 06GL15
[17] Garidel S, Zelsmann M, Chaix N, Voisin P, Boussey J, Beaurain A and Pelissier B 2007 *J. Vac. Sci. Technol.* B **25** 2430
[18] He J, Richter K, Bartha J W and Howitz S 2011 *J. Vac. Sci. Technol.* B **29** 06FC16
[19] Yao C H, Chang C H, Hsieh C W and Sung C K 2010 *Microelectron. Eng.* **87** 864
[20] Choi C-H and Kim C-J 2006 *Nanotechnology* **17** 5326
[21] Morton K J, Nieberg G, Bai S and Chou S Y 2008 *Nanotechnology* **19** 345301
[22] Chang Y F, Chou Q R, Lin J Y and Lee C H 2007 *Appl. Phys.* A **86** 193
[23] Engstrom D and Soh Y 2013 *J. Vac. Sci. Technol.* B **31** 21806
[24] Dimova-Malinovska D, Sendova-Vassileva M, Tzenov N and Kamenova M 1997 *Thin Solid Films* **297** 9
[25] Chartier C, Bastide S and Lévy-Clément C 2008 *Electrochim. Acta* **53** 5509
[26] Huang Z, Geyer N, Werner P, De Boor J and Gösele U 2011 *Adv. Mater.* **23** 285
[27] Li X and Bohn P W 2000 *Appl. Phys. Lett.* **77** 2572
[28] Robinson J T, Evans P G, Liddle J A and Dubon O D 2007 *Nano Lett.* **7** 2009
[29] Oh Y, Choi C, Hong D, Kong S D and Jin S 2012 *Nano Lett.* **12** 2045
[30] Powell O and Harrison H B 2001 *J. Micromech. Microeng.* **11** 217
[31] Seidel H, Csepregi L, Heuberger A and Baumgärtel H 1990 *J. Electrochem. Soc.* **137** 3626
[32] Bean K E 1978 *IEEE Trans. Electron Devices* **25** 1185
[33] Lee S C and Brueck S R J 2004 *J. Vac. Sci. Technol.* B **22** 1949
[34] Li X, Seo H S, Um H D, Jee S W, Cho Y W, Yoo B and Lee J H 2009 *Electrochim. Acta* **54** 6978
[35] Seo H S, Li X, Um H D, Yoo B, Kim J H, Kim K P, Cho Y W and Lee J H 2009 *Mater. Lett.* **63** 2567
[36] Jung J-Y, Guo Z, Jee S-W, Um H-D, Park K-T, Hyun M S, Yang J M and Lee J-H 2010 *Nanotechnology* **21** 445303
[37] Choi K, Song Y, Oh I and Oh J 2015 *RSC Adv.* **5** 76128
[38] Tsujino K and Matsumura M 2005 *Electrochem. Solid-State Lett.* **8** C193
[39] Peng K, Hu J, Yan Y, Wu Y, Fang H, Xu Y, Lee S and Zhu J 2006 *Adv. Funct. Mater.* **16** 387
[40] Lee C-L, Tsujino K, Kanda Y, Ikeda S and Matsumura M 2008 *J. Mater. Chem.* **18** 1015
[41] Huang J, Chiam S Y, Tan H H, Wang S and Chim W K 2010 *Chem. Mater.* **22** 4111
[42] Chang C and Sakdinawat A 2014 *Nat. Commun.* **5** 4243
[43] Tiberio R C, Rooks M J, Chang C, Knollenberg C F, Dobisz E A and Sakdinawat A 2014 *J. Vac. Sci. Technol.* B **32** 06FI01
[44] Shikida M, Sato K, Tokoro K and Uchikawa D 2000 *Sensors Actuators* A **80** 179
[45] Tanaka H, Abe Y, Yoneyama T, Ishikawa J, Takenaka O and Inoue K 2000 *Sensors Actuators* A **82** 270
[46] Tanaka H, Cheng D, Shikida M and Sato K 2006 *Sensors Actuators* A **128** 125